Agronomy Research **19**(S1), 739–748, 2021
https://doi.org/10.15159/AR.21.054

Evaluation of passive cooling system in plywood enclosure for agricultural robot prototype

J. Galins, V. Osadcuks and A. Pecka

Latvia University of Life Sciences and Technologies, Faculty of Engineering, Institute of Energetics, Jana Cakstes boulevard 5, LV-3001 Jelgava, Latvia
*Correspondence: janis.galins@llu.lv

Received: February 1st, 2021; Accepted: March 27th, 2021; Published: April 29th, 2021

Abstract. The use of autonomous robots in agriculture has been increasing rapidly in recent years, but is hampered by the complexity of data recording and processing. The prototyping process involves many changes to the housing design during development. Using laser cutting to make a housing is more convenient, faster and cheaper than milling or casting if only one body needs to be made. To speed up the production of autonomous robot prototypes, the body was made of birch plywood using laser-cut parts. The study analyses the efficiency of passive cooling to make sure that birch wood plywood is suitable for the production of a robotic body for outdoor use in agriculture. Under laboratory conditions, temperature measurements were made inside and outside the housing to determine how the heat released by the electronic components dissipates into the environment. An exponential model with a static coefficient and a time constant can be used to determine the recommended operating time at different ambient temperatures when the allowable operating temperature of the component is known. Air flow and heat transfer simulations were performed to represent heat dissipation. Birch plywood can be used for the production of prototype enclosures for agricultural robots, but the design must provide technological solutions for heat dissipation to prevent overheating of electronic components.

Key words: cooling system, heat transfer, modelling, thermal management.

INTRODUCTION

In the 21st century, the level of human welfare has increased significantly, leading to rising labour costs. In order to reduce production costs, entrepreneurs are forced to use robots to make their products competitive (Marinoudi et al., 2019). Robotic hands are widely used to perform monotonous work, changing the placement of the object. It is much more difficult to create an autonomous robot that collects data and makes decisions itself. Autonomous robots are needed for various agricultural tasks, such as getting rid of the weeds (Xiong et al., 2017; McAllister et al., 2019). The computer vision is associated with the collection and processing of environmental data. Cameras record large amounts of data that are processed by a powerful computer (Malavazi et al., 2018; Le et al., 2019; Raja et al., 2019; Kim et al., 2021). Prototyping of such a robot is associated with many problems:

- Change of location of components during development.
- Data recording and processing emits a significant amount of heat.
- The robot must be waterproof to withstand agricultural conditions such as rain, snow, humidity, temperature fluctuations, UV radiation and aggressive gases.
- Data recording needs to be synchronized before it can be combined.
- The position of each camera must be calibrated before data can be recorded.

Passive cooling without moving parts works more reliably than active cooling. Using a fan for cooling can create additional risks such as dust and dirt getting on the electronics and camera lenses (Lanzerstorfer et al., 2016). Passive and active cooling solutions were compared by Galins et al. (2019) in another study.

3D printers are often used to make prototype housings, but they are not always convenient, fast, or cost-effective. Fused deposition modeling is cheaper and more affordable but the dimensional accuracy of 3D printed part is worse than by stereolithography and selective laser sintering (Minetola & Galati, 2018; Solomon et al., 2020; Zharylkassyn et al., 2020). 3D printing with thermoplastics is very popular in robot prototyping but the use of thermoplastic or plywood impairs heat dissipation in the environment (Flaata et al., 2017; Navarrete & Caldeira, 2019). For larger enclosures, laser-cut acrylic or plywood parts could be used. The mounting platform can be made by CNC milling machine to ensure accurate positioning of the cameras. The study uses thermography, experimental temperature measurements and Solidworks flow simulations to ensure that plywood enclosure is suitable for a prototype of agricultural robot. It is planned to place a bundle of sensors with a computer in a plywood box and to study the heat dissipation in the surrounding environment. The aim of the work is to determine the maximum ambient temperature up to which the equipment can safely operate as well as to determine weak spots of design from thermal point of view.

MATERIALS AND METHODS

The study was developed at the Latvia University of Life Sciences and Technologies, laboratory of the Faculty of Engineering. A prototype agricultural robot was developed that can be used to record and process environmental data (Fig. 1).

The lower body of the robot is used to allow the robot to move on various agricultural road surfaces, as well as in agricultural facilities. Brushed DC motors allow the wheels to move back and forth. The upper part of the body is sensor bundle for environmental data recording and processing (Fig. 2). The sensor bundle should operate in various environmental conditions, including light rain, snow,

Figure 1. Experimental prototype of an agricultural robot: 1 – sensor bundle; 2 – lithium batteries for lower body; 3 – lithium batteries for sensor bundle; 4 – brushed DC motors; 5 – chassis; 6 – wheels.

negative temperatures and direct sunlight. The cameras and computer were placed in a laser-cut birch plywood box to form the upper body. The side parts of the plywood were precisely made to create a finger joint in corners without gaps. Waterproof glue was also used. The body was then coated with urethane varnish to protect the plywood from moisture. Although the upper body was designed to withstand rain, there is a hole in the bottom of the box for safety to drain excess water in the event of a leak. To ensure the stability of the structure, the selected birch plywood thickness is 6 mm. The main advantage of plywood housing for robot prototype is that adjustments can be made easily. Laser-cut parts can be made faster than 3D printed or CNC milled parts. In addition, plywood is a cheaper raw material than plastic or metal. The main disadvantage of such an application is the low thermal conductivity of plywood. The dissipation of heat in the environment was studied. Both experimental temperature measurements and simulations were performed to identify the problem areas. During the experiments, the ambient temperature in the laboratory around the research object was measured.

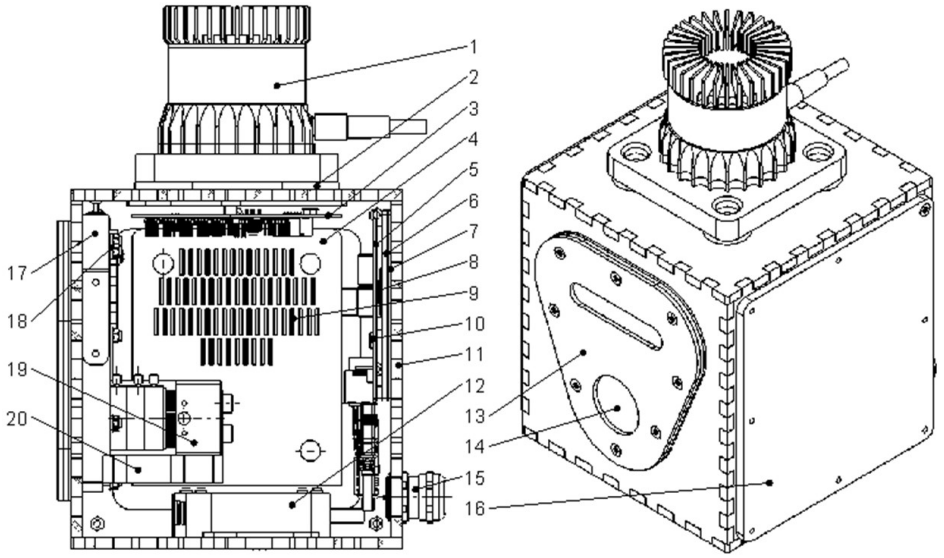

Figure 2. Structure of the research object: 1 – LIDAR; 2 – acrylic standoff; 3 – PCB for sensors; 4 – Wi-Fi router; 5 – PCB for computer; 6 – heatsink for computer; 7 – rubber gasket; 8 – CPU Pentium N4200; 9 – heatsink for Wi-Fi router; 10 – Ethernet controller I211-AT; 11 – plywood enclosure; 12 – adapter for LIDAR; 13 – front cover; 14 – filter for DVS240 camera; 15 – cable gland; 16 – side cover; 17 – calibrating device of records; 18 – depth camera D435; 19 – DVS240 camera; 20 – plywood platform for cameras.

Computational fluid dynamics (CFD) and heat transfer simulations were performed in the Solidworks 2018 software. Each camera must be in a certain position due to the specifics of data processing. Computer board relocation was limited. The simulation model was developed based on experimental temperature measurements, solid

Table 1. Input data for CFD and heat transfer simulations

Parameter	Value	Unit
Gravity in y axis direction	-9.81	m s^{-2}
Atmospheric pressure	10,1325	Pa
Ambient temperature	23	°C
Heat generation rate for computer	4.9–15.4	W
Heat generation rate for LIDAR	13.6	W
Heat generation rate for Wi-Fi router	4.5	W
Fluids type	Air	

materials and environmental conditions. An automatic mesh level with a value of 5 was used. Only conduction and convection without radiation were used for simulated heat transfer. This study uses the same methodology as the previous study on data transmission cooling modelling (Galins et al., 2020). Input data for CFD and heat transfer simulations were selected according to the model equipment and environmental conditions (Table 1).

The results of the simulations are significantly influenced by the thermal conductivity of the selected solid materials (Table 2).

Table 2. Solid materials used for CFD and heat transfer simulations

Part	Size (mm)	Material	Thermal conductivity[1] ($W\ m^{-1}\ K^{-1}$)
LIDAR	110×110×94	Aluminium	~237 (depends on temperature)
Enclosure	188×195×193 (wall thickness 6 mm)	Plywood	0.15
Platform for cameras	140×120×16	Plywood	0.15
Standoff	30×30×4	Acrylic	0.2
PCB for sensors	86×76×1.6	Laminate FR4	0.3
PCB for computer	147×102×1.6	Laminate FR4	0.3
Wi-Fi router	137×114×30	ABS plastic	0.2
Heatsink for Wi-Fi router	130×100×2.5	Aluminium	~237 (depends on temperature)
Heatsink for computer	147×102×3	Aluminium	~237 (depends on temperature)
DVS240 camera	60×40×30	Aluminium	~237 (depends on temperature)
Gasket	147×102×2	Neoprene	0.05
Thermal pad for CPU	12×12×0.5	Silicone	2
CPU	12×12×2	Silicon	~150 (depends on temperature)
Ethernet controllers (2 pcs)	9×9×2	Silicon	~150 (depends on temperature)

[1]Data obtained from (Engineering ToolBox, 2020).

The materials used in the simulations were simplified without taking into account that the thermal conductivity of the material differs in different directions (Yapici et al., 2011). Plywood is not a homogeneous material. There are branched areas with different densities. Moisture content increases the thermal conductivity of wood (Troppová et al., 2015). The thickness tolerance of ± 0.2 mm also has an effect.

DC power supply P3030 was used to measure voltage and current. Voltmeter has an accuracy of ± 0.5% + 3 digits but ammeter ± 1.0% + 3 digits (Advantek Corporation, 2020).

The heating components on printed circuit board (PCB) were identified using a thermal imager testo 868. The thermography camera has an accuracy of ± 2 °C, ± 2% of measurement value. Emissivity can be set from 0.01 to 1 (Testo SE & Co, 2020).

Experimental temperature measurements were made using a data logger GL840 with K type thermocouples. Temperature measurements were taken every second with accuracy of ± 0.05% + 1.0 °C (Graphtec, 2016). Thermocouples were placed both inside and outside the housing.

RESULTS AND DISCUSSION

Heating components were determined by a thermography camera (Fig. 3). The temperature range selected for the thermographic image was 25.6 to 44.0 °C. The thermography picture shows that a significant amount of heat was released by point M1and M2. The visible heat emitters are 2 equal Ethernet controllers I211-AT. The processor was on the other side of the board and could not be accessed by the thermography camera. During the experiment, the CPU temperature was measured with a built-in sensor.

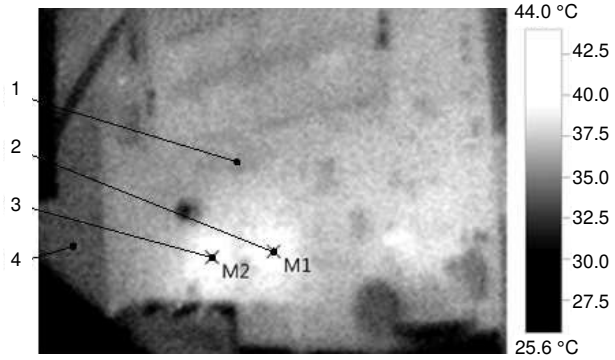

Figure 3. Thermographic image of computer PCB inside the box: 1 – PCB for computer; 2 – Ethernet controller I211-AT; 3 – Ethernet controller I211-AT; 4 – plywood enclosure.

Experimental temperature measurements were made until the system reached steady state. Thermography shows the temperature distribution on the outside of the housing (Fig. 4). In the thermographic image, the highest temperature of 56.2 °C (HS1) was reached on the computer heatsink. Hot spot (HS1) indicates the location of the CPU Pentium N4200 behind the heatsink. At the beginning of the study, it was not clear whether LIDAR could be mounted directly on plywood. HS2 indicates the generation of a significant amount of heat at the bottom of the LIDAR reaching temperature of 55.9 °C. The LIDAR was raised 4 mm above the plywood body to improve bottom cooling by convection. A similar problem would occur if LIDAR would be mounted on a 3D printed thermoplastic housing. The LIDAR has an unequal temperature distribution, because the temperature difference between the point M1 and HS2 was 10.9 °C. The ambient temperature at point M4 is 26.4 °C. It seems that the accuracy of the ambient temperature measurement was significantly affected by the emissivity and the reflected temperature, because in the following measurements with a data logger, the ambient temperature was 3 °C lower. Similar problems in the accuracy of thermographic measurements can be found in other studies (Howell et al., 2020; Zarco-Periñán et al., 2021).

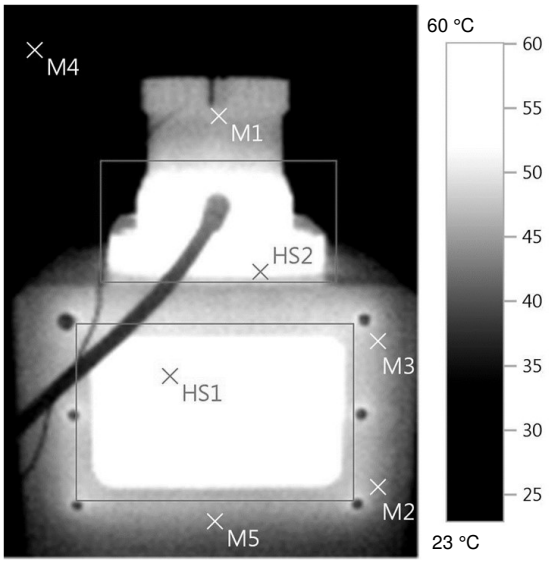

Figure 4. Thermographic image of the research object.

At the bottom of the plywood box, the temperature at points M2 and M5 was 42.4 °C, and at the top at point M3, the temperature was 44.6 °C, thus making a difference of 2.2 °C. This temperature difference is most likely due to the fact that most of the heat is released at the top of the box, although there is some effect on convection.

Dynamic heating curves for different locations were recorded with a logger and thermocouples (Fig. 5).

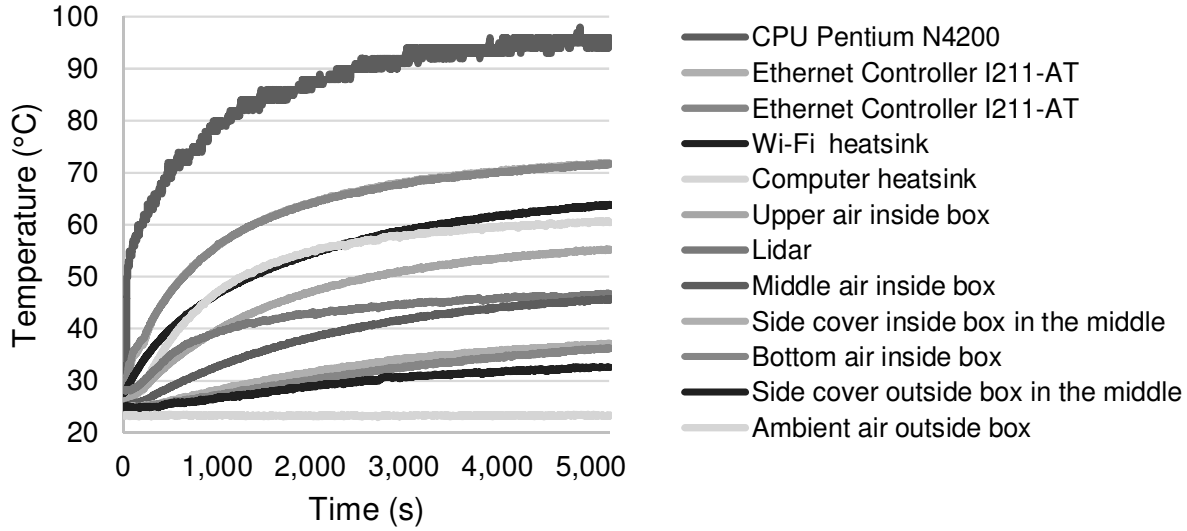

Figure 5. Experimental temperature measurements using thermocouples.

The highest temperature of 96 °C was reached by the CPU Pentium N4200 after 5,000 s. The maximum allowable operating temperature of the processor is 105 °C (Intel Corporation, 2021), thus the critical temperature was not reached. Both Ethernet controllers reached very similar temperatures of about 72 °C thus exceeding the maximum allowable operating temperature of 70 °C (Intel Corporation, 2021). The heatsink of Wi-Fi router reached 64 °C. The problem is that the Wi-Fi router is inside the housing and the heat from the Wi-Fi heatsink is not effectively dissipated to the outside, thus the air temperature in the middle is 46 °C. The upper and bottom air temperature inside the box forms the temperature difference of 18.6 °C. There is no air exchange between inside and outside. The ambient temperature of 23.3 °C was almost constant throughout the experiment. Also the temperature of the side cover inside and outside the box was measured, so that temperature difference of 6 mm thick plywood was 4.6 °C. The computer heatsink heats up to 60.8 °C, which is 4.6 °C more than measured by thermography. This difference could have occurred because the thermocouples were secured with insulating tape, which impaired cooling. The Lidar temperature at the top was 46.3 °C, so it differed from the thermographic reading by only 1.3 °C. Plywood looks like a very good thermal insulator. Thermal conductivity of dry birch plywood SyPly is about 0.15 W m^{-1} K^{-1} (Syktyvkar, 2016).

The simulation shows the air flow trajectory and temperature distribution of the research object (Fig. 6). The temperature distribution represents the heating components and heat dissipation. Air flow trajectories represent passive convection of air.

The heated airflow inside the box moves along the computer board up and then down the middle. The CPU transfers most of the emitted heat through a 0.5 mm thermal pad to the heatsink. It is shown that the Ethernet controller does not have a cooling solution, so the maximum operating temperature of 70 °C was also exceeded. The efficiency of passive cooling can be significantly increased by using finned heatsinks (Hernandez-Perez et al., 2020; Abbas et al., 2021). To improve the cooling of the Ethernet controller, it is necessary to put additional thermal pads between controller and computer heatsink, as well as an additional heatsink with fins directly on the Ethernet controller. An additional large heatsink with fins must be placed on the outside of the computer heatsink to reduce the maximum temperature.

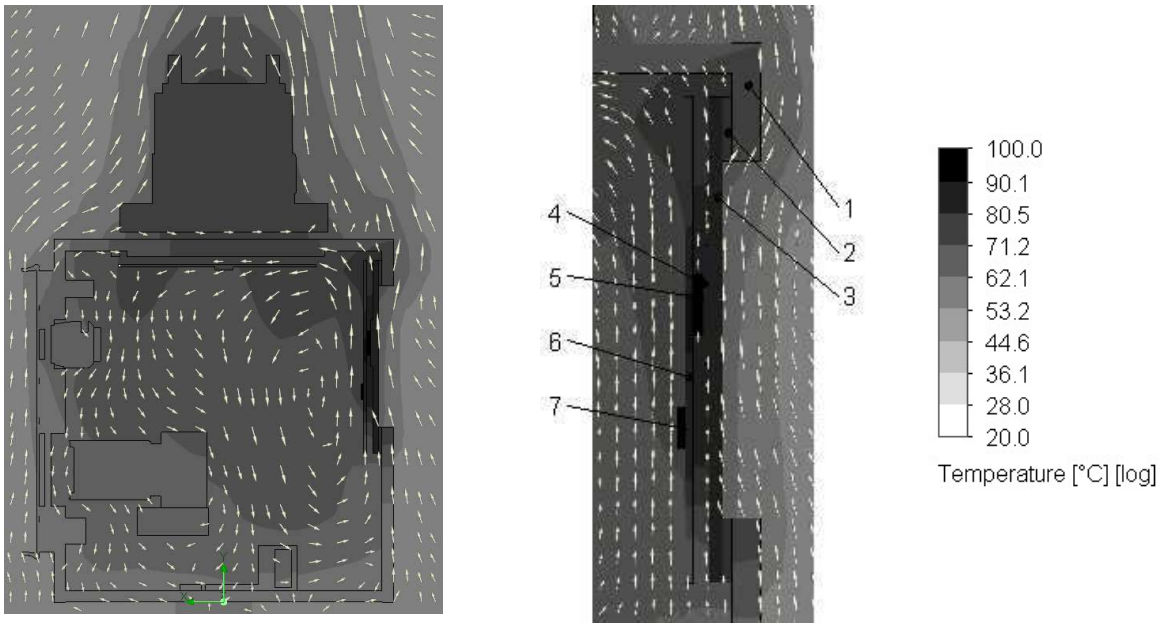

Figure 6. Temperature distribution and airflow trajectories of simulation: 1 – plywood enclosure; 2 – rubber gasket; 3 – heatsink for computer; 4 – thermal pad for CPU; 5 – CPU Pentium N4200; 6 – PCB for computer; 7 – Ethernet controller I211-AT.

The experimental data was used to determine operation time of the sensor bundle in different ambient temperatures. Non-linear least squares analysis (Bates & Chambers, 1992) available in R-statistics package as NLS function. We used exponential model for first order system (1) to fit in experimental data and get static coefficient θ_f, showing final temperature and dynamic coefficient τ showing time when temperature reaches 63% of final temperature.

$$\theta(t) = \theta_f \left(1 - e^{-\frac{t}{\tau}} \right) \tag{1}$$

where $\theta(t)$ – temperature difference above ambient as a function of time; °C; θ_f – static coefficient; °C; t – time, min; τ – time constant, min.

We are interested in temperature differences in relation to ambient temperature, therefore before fitting we subtracted mean ambient temperature value during the experimental run (23.3 °C) from all the measurements. To increase the accuracy of fitting of the coefficients it is recommended to use argument and function measured

numerical values in close magnitudes, so we expressed time in minutes instead of seconds.

Table 3 shows the summary of NLS analysis results. Column θ_f shows static coefficients for different measurement points.

Table 3. Fitted values of coefficients for different measurement points

Measurement point	θ_f, °C	τ, min	Residual standrad error
Lidar	22.3	13.2	0.8929
Ethernet Controller I211-AT	6.7	13.8	1.6680
Ethernet Controller I211-AT	46.5	13.6	1.7760
Wi-Fi heatsink	39.2	19.0	1.5110
Computer heatsink	36.9	17.0	0.4400
Bottom air inside box	17.9	68.1	0.3023
Upper air inside box	32.2	24.2	0.5006
Side cover inside box in the middle	16.2	46.1	0.2628
Side cover outside box in the middle	10.9	45.3	0.3065
Middle air inside box	24.1	34.2	0.2591
CPU Pentium N4200	68.4	7.6	4.8280

Using the Table 3, Eq. 1 and allowable operating temperatures of different components it is possible to determine recommended operation time of the sensor bundle for a given ambient temperature. The best fit was achieved for sensors positioned in air or on large thermal mass objects (LIDAR, large heatsinks), where temperature change was less affected by multiple internal heat sources.

CONCLUSIONS

The study revealed that the current cooling solution is not efficient enough for the unit to operate for a long time at an ambient temperature above 23 °C. Ethernet controller I211-AT exceeded the maximum allowable temperature per 2 °C thus cooling solution needs improvement. The highest temperature of 96 °C was reached by the CPU Pentium N4200 thus not exceeding the maximum allowable operating temperature of 105 °C.

Thermography can be used effectively to identify hot spots where significant amounts of heat are released, but thermocouples should be used for more accurate measurements.

Birch plywood can be used for the production of prototype housings for agricultural robots, but the design must provide technological solutions for heat dissipation to prevent overheating of electronic components.

An exponential model with a static coefficient and a time constant can be used to determine the recommended operating time at different ambient temperatures when the allowable operating temperature of the component is known.

ACKNOWLEDGEMENTS. This research is funded by the Latvian Council of Science, Funding Number: lzp-2018/1-0482.

REFERENCES

Abbas, A., Muneeshwaran, M. & Wang, C.C. 2021. Performance of displaced fin heatsink in natural convection subject to upward and downward arrangement. *International Journal of Thermal Sciences* **162**. doi: 10.1016/j.ijthermalsci.2020.106797

Advantek Corporation. 2020. *P3030 manual*. Available at http://www.advanteks.com/manual_for_P.pdf

Bates, D.M. & Chambers, J.M. 1992. Nonlinear models. Chapter 10 of *Statistical Models in S eds* J. M. Chambers and T. J. Hastie, Wadsworth & Brooks/Cole.

Engineering ToolBox. 2020. Available at https://www.engineeringtoolbox.com/

Flaata, T., Michna, G.J. & Letcher, T. 2017. Thermal conductivity testing apparatus for 3d printed materials. *ASME*. doi: 10.1115/HT2017-4856

Galins, J., Laizans, A. & Galins, A. 2020. Modelling of heat processes for data transmission equipment for operation at high temperature. *Engineering for Rural Development* **19**, 1437–1443. doi: 10.22616/ERDev.2020.19.TF361

Galins, J., Laizans, A. & Galins, A. 2019. Review of cooling solutions for compact electronic devices. *Research for Rural Development* **1**, 201–208. doi: 10.22616/rrd.25.2019.030

Graphtec. 2016. *GL840 Manual*.

Hernandez-Perez, J.G., Carrillo, J.G., Bassam, A., Flota-Banuelos, M. & Patino-Lopez, L.D. 2020. Thermal performance of a discontinuous finned heatsink profile for PV passive cooling. *Applied Thermal Engineering* **184**. doi: 10.1016/j.applthermaleng.2020.116238

Howell, K., Dudek, K. & Soroko, M. 2020. Thermal camera performance and image analysis repeatability in equine thermography. *Infrared Physics and Technology* **110**. doi: 10.1016/j.infrared.2020.103447

Intel Corporation. 2021. Intel Pentium Processor N4200. Available at https://ark.intel.com/content/www/us/en/ark/products/95592/intel-pentium-processor-n4200-2m-cache-up-to-2-5-ghz.html?wapkw=CPU%20Pentium%20N4200%20

Intel Corporation. 2021. Intel Ethernet Controller I211-AT. Available at https://ark.intel.com/content/www/us/en/ark/products/64404/intel-ethernet-controller-i211-at.html

Kim, W.S., Lee, D.H., Kim, Y.J., Kim, T., Lee, W.S. & Choi, C.H. 2021. Stereo-vision-based crop height estimation for agricultural robots. *Computers and Electronics in Agriculture* **181**. doi: 10.1016/j.compag.2020.105937

Lanzerstorfer, C., Neder, F. & Schmied, R. 2016. Constant design air flow industrial ventilation systems with regenerative dust filters: Economic comparison of fan speed-controlled, air damper controlled and uncontrolled operation. *Energy and Buildings* **128**, 503–510. doi: 10.1016/j.enbuild.2016.07.032

Le, T., Omholt-Gjevestad, J.G. & From, P.J. 2019. Online 3D Mapping and Localization System for Agricultural Robots. *IFAC-PapersOnLine* **52**(30), 167–172. doi: 10.1016/j.ifacol.2019.12.516

Malavazi, F.B.P., Guyonneau, R., Fasquel, J.B., Lagrange, S. & Mercier, F. 2018. LiDAR-only based navigation algorithm for an autonomous agricultural robot. *Computers and Electronics in Agriculture* **154**, 71–79. doi: 10.1016/j.compag.2018.08.034

Marinoudi, V., Sørensen, C.G., Pearson, S. & Bochtis, D. 2019. Robotics and labour in agriculture. A context consideration. *Biosystems Engineering* **184**, 111–121. doi: 10.1016/j.biosystemseng.2019.06.013

McAllister, W., Osipychev, D., Davis, A. & Chowdhary, G. 2019. Agbots: Weeding a field with a team of autonomous robots. *Computers and Electronics in Agriculture* **163**. doi: 10.1016/j.compag.2019.05.036

Minetola, P. & Galati, M. 2018. A challenge for enhancing the dimensional accuracy of a low-cost 3D printer by means of self-replicated parts. *Additive Manufacturing* **22**, 256–264. doi: 10.1016/j.addma.2018.05.028

Navarrete, M.J.I. & Caldeira, T. 2019. Smart Manufacturing of 3D Printed Robots. *Advances in Science and Engineering Technology*, 1–5 doi: 10.1109/ICASET.2019.8714537

Raja, R., Slaughter, D.C., Fennimore, S.A., Nguyen, T.T., Vuong, V.L., Sinha, N. & Siemens, M.C. 2019. Crop signalling: A novel crop recognition technique for robotic weed control. *Biosystems Engineering* **187**, 278–291. doi: 10.1016/j.biosystemseng.2019.09.011

Solomon, I.J., Sevvel, P. & Gunasekaran, J. 2020. A review on the various processing parameters in FDM. *Materials Today: Proceedings*, pp. 10–15. doi: 10.1016/j.matpr.2020.05.484

Syktyvkar Plywood Mill. 2016. Handbook SyPly. Available at https://hanson-plywood.co.uk/wp-content/uploads/2017/07/SyPly_handbook_ENG2016.pdf

Testo SE & Co. 2020. Data Sheet Testo 868, pp. 4.

Troppová, E., Švehlík, M., Tippner, J. & Wimmer, R. 2015. Influence of temperature and moisture content on the thermal conductivity of wood-based fibreboards. *Materials and Structures/Materiaux et Constructions* **48**(12), 4077–4083. doi: 10.1617/s11527-014-0467-4

Xiong, Y., Ge, Y., Liang, Y. & Blackmore, S. 2017. Development of a prototype robot and fast path-planning algorithm for static laser weeding. *Computers and Electronics in Agriculture* **142**, 494–503. doi: 10.1016/j.compag.2017.11.023

Yapici, F., Ozcifci, A., Esen, R. & Kurt, S. 2011. The effect of grain angle and species on thermal conductivity of some selected wood species. *BioResources* **6**(3), 2757–2762. doi: 10.15376/biores.6.3.2757-2762

Zarco-Periñán, P.J., Martínez-Ramos, J.L. & Zarco-Soto, F.J. 2021. A novel method to correct temperature problems revealed by infrared thermography in electrical substations. *Infrared Physics and Technology* **113**. doi: 10.1016/j.infrared.2020.103623

Zharylkassyn, B., Perveen, A. & Talamona, D. 2020. Effect of process parameters and materials on the dimensional accuracy of FDM parts. *Materials Today: Proceedings*. doi: 10.1016/j.matpr.2020.11.332